energies

Article

DC-DC Boost Converter with Reduced Switching Losses in Wide Range of Voltage Gain

Andrzej Mondzik [1,*], Stanisław Piróg [1], Robert Stala [1], Adam Penczek [1] and Piotr Gucwa [2]

[1] Department of Power Electronics and Energy Control Systems, Faculty of Electrical Engineering, Automatics, Computer Science and Biomedical Engineering, AGH University of Science and Technology, Al. Mickiewicza 30, 30-059 Krakow, Poland; pirog@agh.edu.pl (S.P.); stala@agh.edu.pl (R.S.); penczek@agh.edu.pl (A.P.)

[2] Research and Development, SMA-Magnetics Sp. z o.o., Komandosów 3/1, 32-085 Modlniczka, Poland; piotr.gucwa@sma-magnetics.com

* Correspondence: mondzik@agh.edu.pl

Abstract: This article presents the results of research on a new topology of a DC-DC converter in which switching losses are reduced by an auxiliary switching circuit (ASC). The proposed ASC can work as a passive or active circuit depending on the voltage gain of the converter. In both cases, this does not affect the operation of the main circuit and is analogous to a classic boost converter, which allows the use of the same control circuits and methods. The operation of the ASC is synchronized with the control of the main converter transistor. The reduction of transistor turn-off losses over a wide range of converter gain is a unique advantage of the proposed auxiliary circuit. This is evidenced by the comparison of the loss reduction with the classic boost converter and the reference converter with soft turn off. This article presents an in-depth analytical discussion related to the reduction of power losses, supported by simulation results, and verified experimentally.

Keywords: DC-DC converter; boost converter; high efficiency; ZVS converter; ZVT

check for updates

Citation: Mondzik, A.; Piróg, S.; Stala, R.; Penczek, A.; Gucwa, P. DC-DC Boost Converter with Reduced Switching Losses in Wide Range of Voltage Gain. *Energies* **2023**, *16*, 4397. https://doi.org/10.3390/en16114397

Academic Editor: Miguel Castilla

Received: 18 April 2023
Revised: 25 May 2023
Accepted: 26 May 2023
Published: 29 May 2023

1. Introduction

A DC-DC boost converter is a solution of great importance in applications with a noninsulated power supply and power factor correction (PFC) systems [1]. The converter can be used in a wide range of applications and can be designed to use different types of switches, including IGBTs. IGBTs remain a very advantageous solution considering the cost-per-watt calculation in the appropriate frequency range. Therefore, IGBT switches with a rated voltage of 650 V can be found in single-phase applications with front PFCs, such as on-line uninterruptible power supplies (UPSs) or AC-AC drive systems.

An important portion of boost converter power losses are associated with its turn-off process. However, they can be reduced by implementing soft switching. The publication [2] presents an analysis of the soft switching process of an IGBT transistor and shows that it allows the reduction of power losses in the boost converter.

The reduction of switching losses can be achieved by using low-complex additional circuits implemented in a classic converter. The switching turn-off loss decrease based on the idea of an auxiliary switching cell (ASC), which reduces the voltage rise across the transistor (du_{DS}/dt), was demonstrated in three-level neutral-point-clamped (NPC) inverters (VSI) in [3]. In [4], the method for turn-off loss reduction was demonstrated in a boost converter with auxiliary circuits. The principle of turn-off loss reduction, proposed in [4], assumes that the rate of increase in the U_{CE} collector–emitter voltage during the shutdown of the transistor is slow enough to complete the current commutation with a low part of the power loss. The increase in U_{CE} voltage is reduced by an additional capacitor charged to the output voltage before the shutdown process. The optimal voltage value across the auxiliary capacitor is at the level of the output voltage. These conditions are obtained when the converter shown in [4] operates with a voltage gain of less than double.

At higher gain, the boost converter presented in [4] requires other auxiliary circuits to achieve effective reduction of turn-off losses. The implementation of the ASC concept for a DC-DC converter has been demonstrated in [4] and previously in patents [5–7]. An advantageous feature of the system proposed in [4] is its relatively simple ASC system, consisting of two diodes and an auxiliary capacitor and inductor. However, for voltage amplification greater than two, such passive ASC does not provide optimal conditions to reduce switching losses.

In a boost topology, the soft switching technique can be achieved by implementing different kinds of auxiliary commutation circuits and control [8–34]. The concepts presented in the literature [8–14] are based on the use of passive auxiliary circuits. The implementation of soft switching in a suitable controlled interleaved circuit with output capacitances of transistors is shown in [8–11]. In [8], soft switching operation in boundary conduction mode (BCM) was demonstrated, and in [9], ZVS near the critical conduction mode (CRM). In the DC-DC converter presented in [10], the current of inductors is continuous to achieve ZVS in an auxiliary inductor.

Publications [12,13] present auxiliary circuits based on L, C elements and diodes using resonant circuits. These circuits are characterized by a low number of elements and low complexity. However, some inductive elements are located in the power circuit in series with the transistor. The snubber system shown in [14] provides the zero-voltage transition (ZVS) and zero-current switching (ZCS) of the boost converter. The circuit uses a capacitor, coupled chokes, and diodes, and the inductive element and diode are placed in the converter power circuit.

Publications [15–34] present concepts for the implementation of zero-voltage commutation (ZVT) in a boost converter with auxiliary circuits, controlled by switches and diodes. In the area of these active systems, solutions based on circuits containing transistors and diodes, as well as the L and C passive components, are also used. Magnetically coupled elements [19–23] are also implemented in active auxiliary circuits for ZVT which may require a more complex design approach. In [24–29], resonant circuits are also implemented in active auxiliary circuits for ZVT where [24–27] demonstrate development of a ZVT snubber topology, [28] an auxiliary resonant circuit configured in H-bridge, and [29] a concept of topology characterized by low-voltage ringing.

Soft-switching operation in a PWM DC-DC boost converter can be also achieved with the implementation of switched-capacitor-based (SC) circuits [30,31]. In [30], the operation of a boost converter with a capacitor-switched snubber attached is demonstrated. The snubber circuit is achieved without any inductive components which is a benefit of some SC circuits. In [31], a converter with embedded SC circuits and its soft-switching ability is demonstrated.

Since the boost topology is a typical part of PFC rectifiers, active snubbers allow a reduction in switching losses in PFC systems as well, which is demonstrated in [32–34].

The soft-switching concept method proposed in this paper is based on an active ASC system where improved conditions for the soft shutdown of the transistor over a large range of output voltage regulation are achieved. Compared to the converter capabilities presented in [4], the proposed system allows for the effective reduction of turn-off losses for a larger voltage gain range (also for $G > 2$). The investigated converter uses an active auxiliary circuit with low complexity and simple control, which is a beneficial feature of this solution. The presented method can be used in a continuous conduction model (CCM) as well as in a discontinuous conduction mode (DCM) of the boost converter operation at variable duty cycles and it does not require regulation of the switching frequency when the load varies. The proposed system improves the parameters of the converter proposed in [4]. It uses the analogous concept of reducing the rate of voltage increase across the transistor and the auxiliary discharge circuit of the auxiliary capacitor. However, a new active circuit and control method for auxiliary capacitor charging is proposed, supporting the operation of the system presented in [4], which improves the ZVT for $G > 2$.

This article is organized as follows. Section 2 demonstrates the concept of the proposed circuit and control method for soft switching in the boost converter. Section 3 presents analyses related to the selection of converter parameters, and Section 4 presents experimental results with waveforms and measured efficiency.

2. Principle of Operation

The proposed DC-DC boost converter is presented in Figure 1. The operation of the power circuit of the converter is the same as in the classic boost DC-DC converter. The voltage gain (U_{out}/U_{in}) depends on the duty cycle of the main transistor switching.

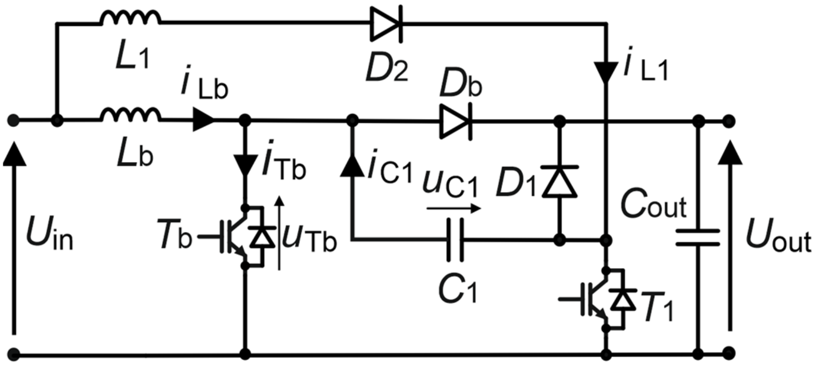

Figure 1. The proposed DC-DC boost converter with the auxiliary switching circuit.

In the proposed boost converter (Figure 1), the auxiliary circuits composed of the devices T_1, D_1, D_2, C_1, and L_1 are used for soft-switching implementation. The soft switching is achieved in the proposed circuit when the voltage across the main transistor rises slowly enough to reduce turn-off losses (Figure 2). The function of the auxiliary circuit components is described in Table 1.

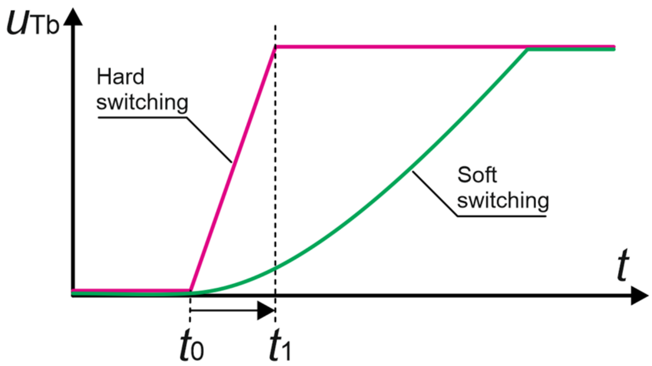

Figure 2. Voltage across the T_b transistor at its turnoff—the purpose of the soft turn-off concept implementation.

Table 1. Function of components used in auxiliary circuits.

Component	Function
C_1	The capacitor which decelerates voltage rise across the T_b transistor during its turn off
D_1	The diode activated during T_b turn-off process
L_1, D_2	Components of the C_1 capacitor charging circuit
T_1	The transistor which improves C_1 capacitor charging, by the L_1 current control

2.1. Zero-Voltage-Switching ZVS of Turn-Off Condition

Figure 3 presents stages of operation in the converter when the main transistor is turned off. In the proposed circuit, ZVS occurs during the turning off of the main transistor T_b. From Figure 3 it can be seen that voltage across the T_b is:

$$u_{Tb} = u_{out} - u_{C1}, \tag{1}$$

where u_{out} is the output voltage and u_{C1} is the voltage across the capacitor C_1.

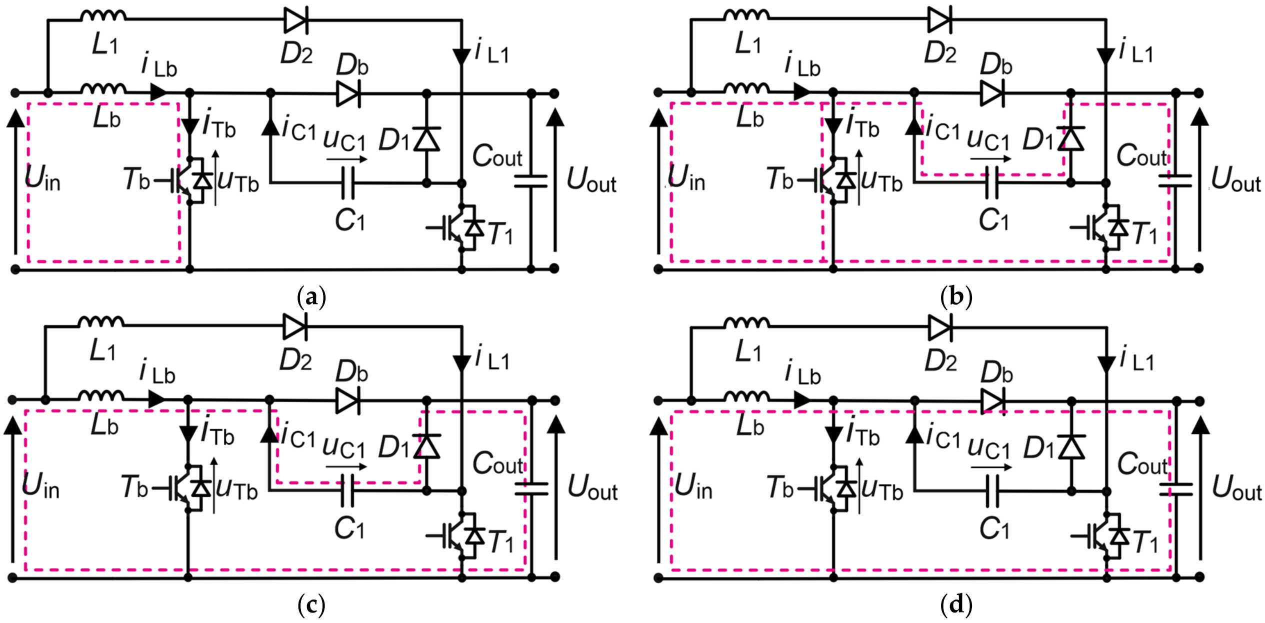

Figure 3. Stages of operation at T_b transistor turn-off with ZVS in the proposed converter. (**a**) state before turn-off of transistor T_b, (**b**) start of turn-off T_b, (**c**) discharge of the auxiliary capacitor, (**d**) state after turn-off of the transistor.

If the capacitor C_1 is charged to the output voltage, the slow voltage rise across the T_b transistor starts at zero, which creates optimal conditions for ZVS operation (at the time-point indicated as t_0 in Figure 2):

$$u_{Tb}(t_0) = 0, \text{ when } u_{C1}(t_0) = u_{out}, \tag{2}$$

where $u_{Tb}(t_0)$ and $u_{C1}(t_0)$ is the voltage across the transistor T_b and the capacitor C_1 at the time-point t_0.

ZVS turn-off is not achieved when the C_1 capacitor voltage is below the output voltage level at beginning of T_b turn-off.

$$u_{Tb}(t_0) > 0, \text{ when } u_{C1}(t_0) < u_{out}, \tag{3}$$

Figure 4 presents model waveforms at the turn off of the T_b transistor in the boost converter in the case when the auxiliary capacitor is properly charged (Figure 4a) and when its charging is below the output voltage level (Figure 4b).

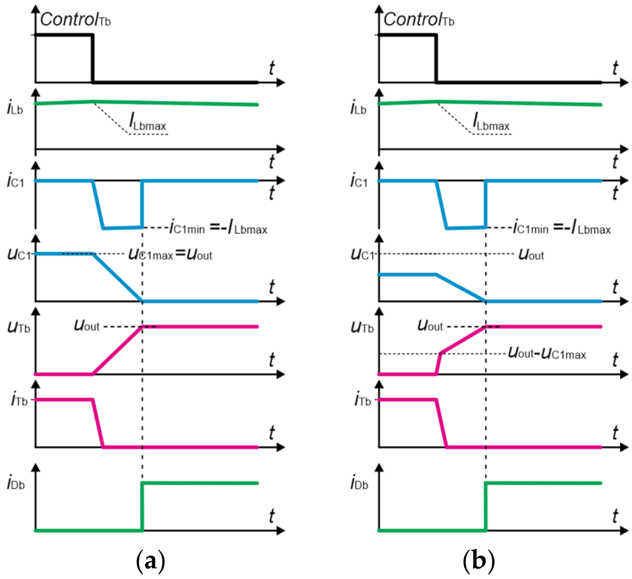

Figure 4. (**a**) Ideal ZVS at the turn off of the T_b transistor, and (**b**) nonideal ZVS process in the converter presented in [4].

2.2. Optimal ZVS Conditions

The proposed converter contains the circuit which allows for auxiliary capacitor C_1 charging. The charging circuit is composed of the resonant choke L_1, the C_1 capacitor, diodes D_2, and components of the power circuit T_b as well as the active component T_1. When the T_1 transistor is not used, the C_1 capacitor is charged from the input voltage in an oscillatory circuit to the following value:

$$u_{\mathrm{C1max}} = 2(U_{\mathrm{in}} - u_{\mathrm{C1init}}), \quad (4)$$

where U_{in} is the supply voltage, and u_{C1max} and u_{C1init} is the maximum and initial voltage of the capacitor C_1.

At rated conditions, the initial voltage of the C_1 capacitor is zero and the capacitor can be charged to $2U_{\mathrm{in}}$. In such a case, the ZVS conditions may not be assured for two following reasons:

- The converter operates with voltage gain $G > 2$. In such a case, the maximal voltage across the C_1 capacitor is below the output voltage: $u_{\mathrm{C1max}} = 2U_{\mathrm{in}}(t_0) < \mathrm{G}U_{\mathrm{in}}$. Assuming low voltage ripple across the input capacitor, this relationship can be simplified to the following form: $u_{\mathrm{C1max}} = 2U_{\mathrm{in}} < \mathrm{G}U_{\mathrm{in}}$.
- Nonzero initial voltage in the C_1 capacitor charging process. This can occur when the converter operates in a light load and therefore has insignificant importance from an efficiency optimization viewpoint.

Therefore, the ZVS conditions are not accomplished in the case where the converter operates with voltage gain $G > 2$ when C_1 capacitor is charging with the use of an auxiliary diode-inductor circuit (D_2, L_1). To create fair ZVS conditions for T_b, an active C_1 capacitor charging circuit can be used. The active charging circuit utilizes an additional T_1 transistor along with D_2, L_1 components.

2.3. The Active Auxiliary Circuit for ZVS Operation

Operation of the active auxiliary charging circuit assumes the use of the T_1 transistor to improve C_1 capacitor charging through an increase in the initial current of the L_1 inductor. This leads to an increase in the charging voltage of capacitor C_1 to meet the conditions of ZVS in the system (2).

Figure 5 shows the idealized waveforms related to the operation of an auxiliary circuit with the transistor T_1 to obtain a nonzero value of the initial current when charging the capacitor C_1. During this process of charging the C_1 capacitor, the following stages are used:

- Stage 1 (Figure 6b): the main switch T_b is turned on along with the T_1 transistor. The C_1 capacitor is not charged in this state, but the current of the L_1 inductor rises.
- Stage 2 (Figure 6c): after a sufficient time, the transistor T_1 is switched off and the process of charging C_1 from the nonzero initial current conditions in the L_1 choke begins. The switching time of transistor T_1 is much shorter than the half-period of the pulse of the main transistor T_b.

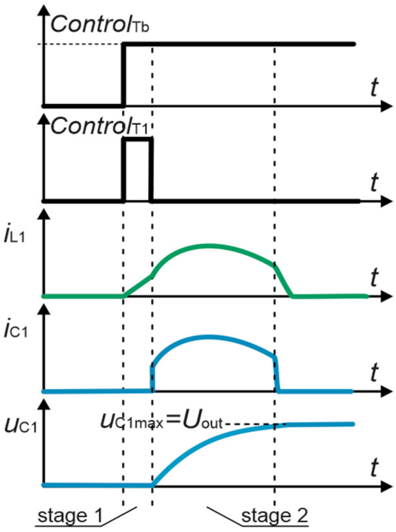

Figure 5. Model of the C_1 capacitor charging process in the proposed converter.

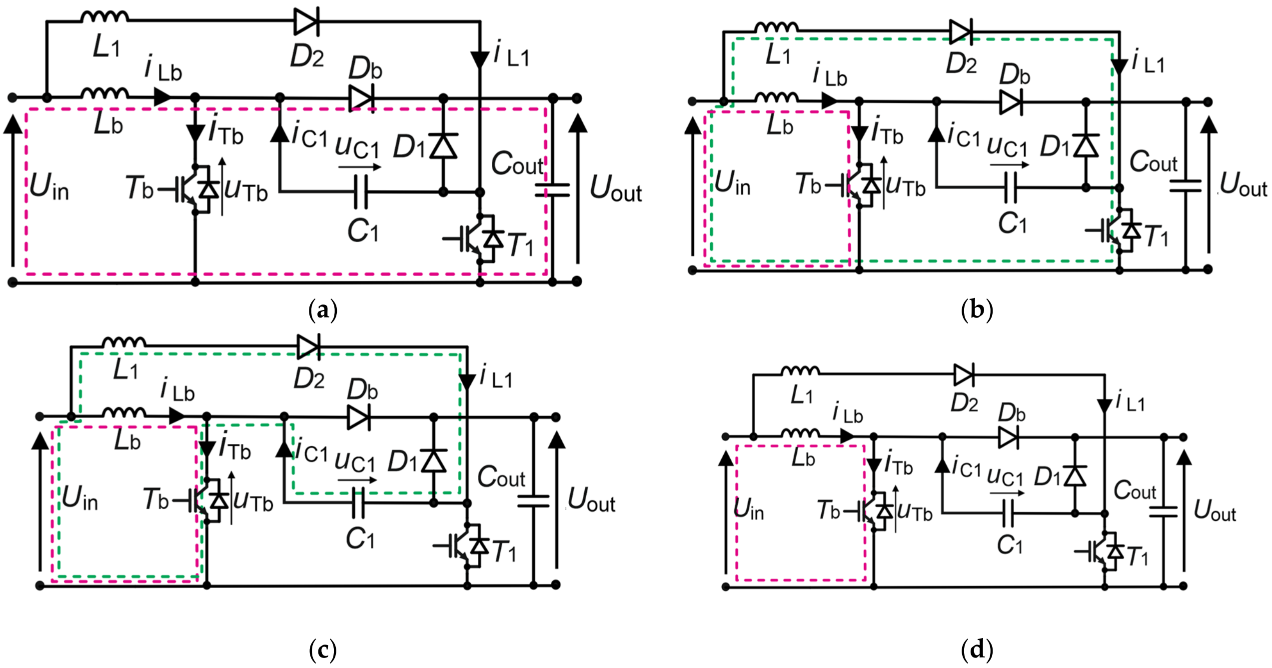

Figure 6. Stages of operation at T_b transistor turn-on. Controlled charging of the C_1 capacitor by the T_1 transistor in the proposed converter. (**a**) State before turn-on of transistor T_b (**b**) the T_1 transistor turn-on for control of the current of the L_1 inductor rise, (**c**) the process of C_1 capacitor charging. The switching time of transistor T_1 is much shorter than the half-period of the pulse of the main transistor T_b, (**d**) state after turn-on of transistor T_b.

The charging of C_1 is continued in the resonant circuit and after the charge current (i_{L1}) disappears, the converter remains in the typical main circuit state, in which the main transistor T_b is switched on (Figure 6d). The process of the C_1 capacitor is controlled in the same way in CCM and DCM modes of operation.

3. Parameters of Auxiliary Circuit Devices and Control

The capacitance of the auxiliary capacitor C_1 determines collector–emitter voltage rise across the T_b transistor (du_{Tb}/dt—Figure 4). Directly after the T_b is turned off, the inductor L_b current (i_{L1}) flows through the C_1 capacitor. During this time interval the C_1 is being discharged and the voltage across the T_b transistors rises according to (1) (Figure 4). Assuming a constant value of the inductor's current during the commutation time interval, the u_{C1} voltage derivative is the following:

$$du_{C1}/dt = \frac{I_{Lb}}{C_1}, \tag{5}$$

where I_{Lb} is the average L_b inductor's current during the time when the C_1 capacitor is discharging (for $u_{Tb} < U_{in}$ the inductor's current is still rising, therefore the current I_{Lb} is slightly below the maximum I_{Lbm}; however, for the model of capacitor selection it can be assumed that $I_{Lb} = I_{Lm}$).

At rated conditions, the C_1 capacitor is charged to the output voltage. Therefore, the C_1 capacitance is selected according to the following formula:

$$C_1 = \frac{I_{Lm}}{U_{out}} t_C, \tag{6}$$

where t_C is the time period when the C_1 capacitor is discharging (Figure 3c).

The I_{Lm} and U_{out} are determined by design requirements, but the time interval when u_{C1} rises is set based on the rate of switching-losses reduction.

The most critical issue for the ZVS operation of the converter is the C_1 capacitor charging process. The C_1 capacitor is charged from the input voltage source. When the voltage gain of the converter is $G_U > 2$, the C_1 capacitor must be charged with the use of the auxiliary active circuit which allows it to achieve the optimal ZVS conditions:

$$U_{C1m} = U_{out}, \tag{7}$$

The charging of the C_1 capacitor starts by switching the transistor T_1 simultaneously with the transistor T_b. As a result, the L_1 choke current increases to (Figures 5 and 6) the value:

$$I_{L1lmax} = \frac{U_{in}}{L_1} t_1, \tag{8}$$

where t_1 is the time when the transistor T_1 is switched on.

In the next stage, after switching off the transistor T_1, the capacitor C_1 is charged in a circuit composed of elements L_1, D_2, C_1, and T_b, with initial current conditions $I_0 = I_{L1max}$, and voltage U_{C10} which should be rated 0. The waveform of the voltage across the capacitor and its current, for the given initial conditions, is described by the following relationships:

$$u_{C1} = U_{in}[1 - cos(\omega_{o1} t)] + I_0 \rho_1 sin(\omega_1 t), \tag{9}$$

$$i_{C1} = I_0 cos(\omega_{o1} t) + \frac{U_{in}}{\rho_1} sin(\omega_1 t), \tag{10}$$

$$\rho_1 = \sqrt{\frac{L_1}{C_1}}, \omega_{o1} = \frac{1}{\sqrt{L_1 C_1}}, \tag{11}$$

The charging ends after one oscillation time, i.e., for $\omega_{o1}t = \pi$. It denotes that the capacitor C_1 is charged to the value:

$$U_{C1max} = U_{in} + I_0\rho_1, \tag{12}$$

The initial condition of the C_1 capacitor charging current, assuming that the capacitor should be charged to the value of the output voltage, is the following:

$$U_{in} + I_0\rho_1 = U_{out} \Rightarrow I_0 = \frac{U_{out} - U_{in}}{\rho_1}, \tag{13}$$

The duration of the switching pulse of the transistor T_1, in which the choke L_1 current increases linearly, should be as follows:

$$\frac{U_{in}}{L_1}t_l = \frac{U_{out} - U_{in}}{\rho_1} \Rightarrow t_l \geq \frac{U_{out} - U_{in}}{U_{in}}\frac{\sqrt{C_1}}{L_1}, \tag{14}$$

For the converter's voltage gain $G_U = \frac{U_{out}}{U_{in}}$ the relationship (14) can be expressed in the following form:

$$t_l \geq (G_U - 1)\frac{\sqrt{C_1}}{L_1} \tag{15}$$

From Equation (15), it follows that the duration of the T_1 transistor on-state pulse-switching varies along with the voltage gain of the converter. However, it can be tuned using the relation (15) and feedback from the duty cycle or the voltage gain measurement.

The use of the ASC system does not change the voltage stress across the transistor and the diode in the power circuit of the converter $U_{\mathrm{Tbm}} = U_{\mathrm{Dbm}} = U_{\mathrm{out}}$. Based on the analysis of the operating stages of the system shown in Figures 3 and 6, it also follows that the voltage stress across the active elements T_1 and D_1 of the ASC circuit is also equal to the value of the output voltage. Voltage stress across the D_2 diode reaches the value equal to a difference in output and input voltage. The stages of operation from which this follows are shown in Table 2.

Table 2. Voltage stress across devices in the proposed converter.

Device	T_{b}	D_{b}	T_1	D_1	D_2	L_1	L_1
Maximum voltage across the device	U_{out} Figure 3d	U_{out} Figure 3a	U_{out} Figure 3b	U_{out} Figure 6b	$U_{\mathrm{out}} - U_{\mathrm{in}}$ Figure 3c	$U_{\mathrm{max}} = U_{\mathrm{in}}$ Figure 6b	$U_{\mathrm{min}} = U_{\mathrm{in}} - U_{\mathrm{out}}$ Figure 6c

4. Experimental Results

The new concept of the boost system with soft turn-off and the efficiency of the converter have been experimentally verified. Table 3 lists semiconductor and passive components used in experimental systems, while Figure 7 shows a photograph of the laboratory setup.

Table 3. Parameters of the main components of the tested converters.

Component	**Type**
T_{b}	RJH65T46DPQ-A0,
D_{b}	SCS240KE2HR
D_1, D_2	RFN10BM6SFHTL
Passives	L_{b} = 150 uH, C_{out} = 9.4 uF, C_1 = 44 nF, L_1 = 80 uH

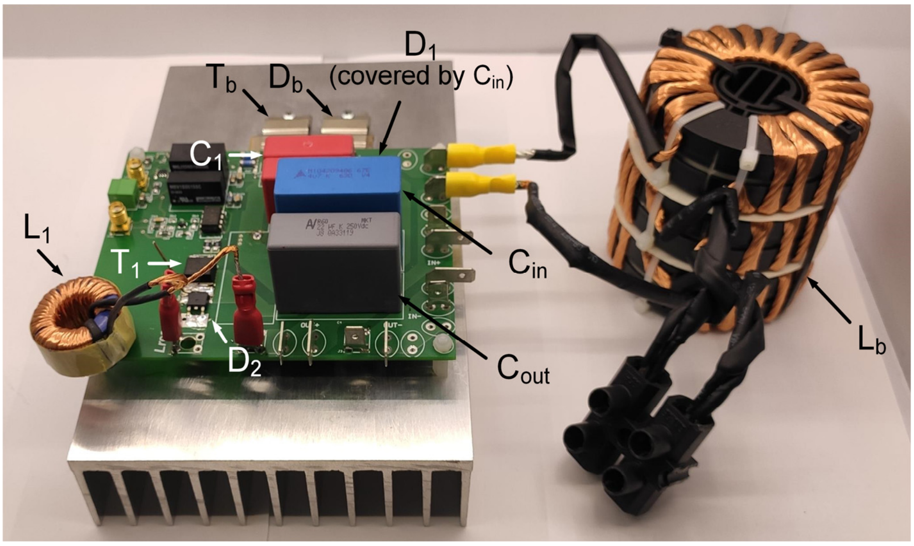

Figure 7. The laboratory setup for tests of the proposed converter, and two other established types of a boost converter.

The supply voltage of the converter was set at the level of U_{in} = 100 V, with the output at the level of U_{out} = 400 V, so that it was possible to inspect the operation of the proposed system at high gain. The tests were carried out for different switching frequencies of the transistor and load power up to 3.5 kW. The maximum junction temperature of the semiconductor elements used are typical (150 °C and 175 °C).

Figure 8 shows a set of waveforms demonstrating the operation of the system according to the soft switching concept. These results show that the main current waveform of the converter choke is analogous to that of a classic boost converter. The current of the auxiliary choke increases linearly in the first stage after switching on the transistor T_b, and then participates in the oscillation charging the capacitor C_1. In the current waveform of capacitor C_1, its charging with nonzero initial current conditions and discharge with the main choke current L_b are seen. Similarly, the correct operation of the soft-switching circuits can be determined from the DCM waveforms shown in Figure 9. The waveforms shown in Figure 10 demonstrate the effectiveness of the applied loss-reduction concept when the transistor is turned off in the boost converter for $G_U > 2$ gain. The proposed system slows down the collector–emitter voltage across the T_b transistor and the improvement over [4] is very clear. Of course, this is also a solution that significantly reduces switching losses compared to the classic boost system. In the tests, the results of which are shown in Figures 8 and 9, the transistors T_b and T_1 are switched on simultaneously (in the time-instant where the drain-source voltage of Tb falls down), and when the T_1 transistor is turned off the C_1 current starts to flow and the C_1 capacitor is charged.

The efficiency measurements confirm the reduction of energy losses by applying the soft turn-off concept, as shown in Figures 11–13. The proposed converter efficiency is compared to the classic boost converter and the converter presented in [4]. In all cases, results of efficiency were achieved in the same basic setup for the voltage gain G_U = 4; thus, this article also expands the knowledge of the system studied in the literature [4]. Figures 11 and 12 present results of efficiency versus power at 32.2 kHz and 48.7 kHz according to typical characteristics, while the results shown in Figure 13 show the efficiency relationship versus switching frequency. From the results presented in Figures 11–13 it can be seen that the proposed system is more efficient than both the boost converter and the concept from [4].

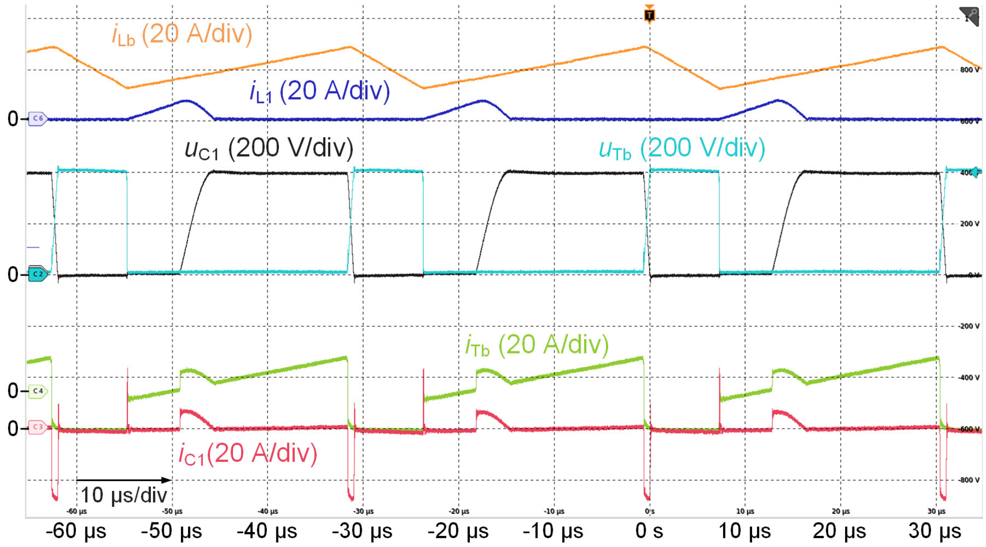

Figure 8. Steady-state waveforms of the proposed converter at CCM: 1—u_{C1}, 2—u_{Tb}, 3—i_{C1}, 4—i_{Tb}, 5—i_{Lb}, 6—i_{L1} at switching frequency f_{sw}= 32.2 kHz, the gain G_U = 4 (U_{in} = 100 V, U_{out} = 400 V), P_{out} = 2 kW. 20 A/div, 200 V/div, 10 us/div.

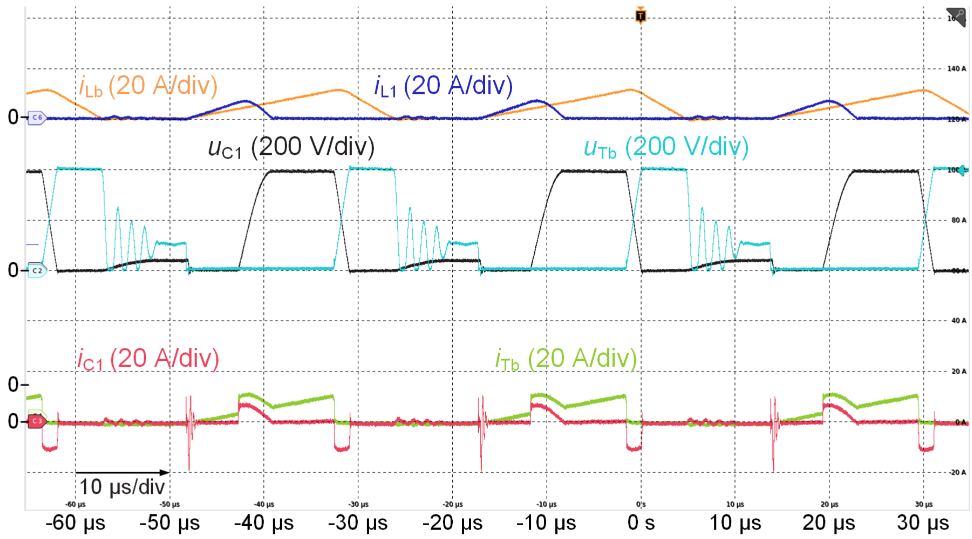

Figure 9. Steady-state waveforms of the proposed converter at DCM: 1—u_{C1}, 2—u_{Tb}, 3—i_{C1}, 4—i_{Tb}, 5—i_{Lb}, 6—i_{L1} at switching frequency f_{sw}=32.2 kHz, the gain G_U = 4 (U_{in} = 100 V, U_{out} = 400 V), P_{out} = 0.5 kW. 20 A/div, 200 V/div, 10 us/div.

The difference becomes greater as the switching frequency increases, which creates greater possibilities for designing boost converters with a higher switching frequency and smaller volume of passive components. The ASC system introduces additional switching losses, as can be seen in the results shown in the Figure 12 where, for low power, the proposed system is less efficient than the converter shown in [4]. However, the switching losses of the ASC circuit are so insignificant that at 2kW increasing the switching frequency is beneficial for the proposed system (Figure 13).

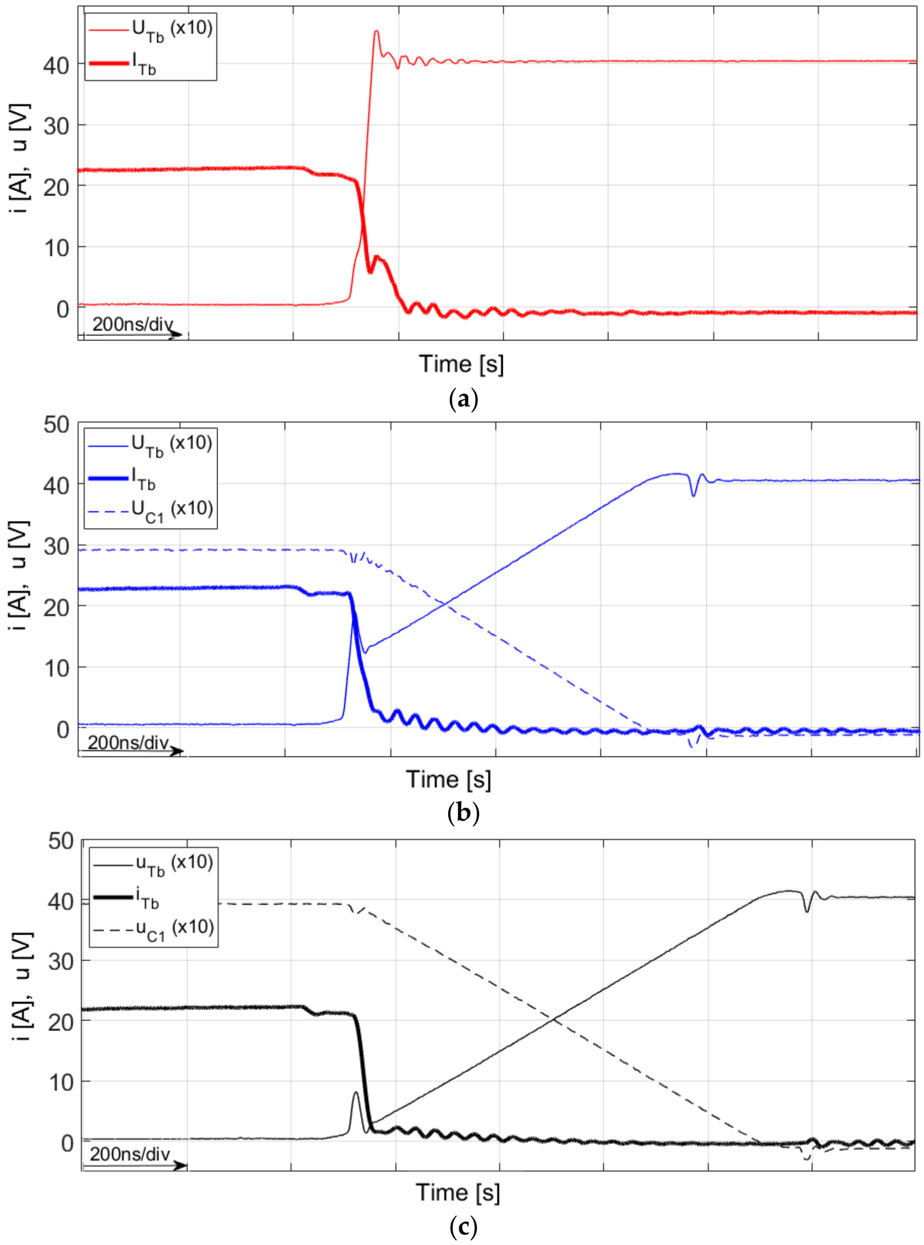

Figure 10. Current (10 A/div) and voltage (100 V/div) waveforms during the turn-off process of the T_b transistor in the boost converter (**a**), the converter from Ref. [4] (**b**), and the proposed (**c**) at P_{out} = 2 kW, U_{in} = 150 V, U_{out} = 400 V. Experimental results plotted using MATLAB software.

Figure 14 presents a thermal photo of the proposed laboratory converter. The recording was performed with a Flir E96 thermal imaging camera. The parameters of the camera were: resolution 640 × 480, emissivity 0.98, and range of temperature from −20 °C to +120 °C. The reflected and the ambient temperature was 20 °C. The converter and chokes were placed on a nonreflective rubber bench mat. The measurement was performed from approximately 1 m distance using neutral white LED light illumination. The measurements were made in steady state for supply voltage U_{in} = 100 V, output power P_{out} = 2 kW, and pulse frequency f_{sw} = 32.2 kHz. The output voltage was 400 V. The highest temperature occured on the transistor T_b and was about 60 °C. Another element with a noticeable temperature of about 35 °C was the diode D_1. The temperature of the remaining elements did not exceed 30 °C. Figure 14 exhibits that the power losses of the boost elements outside the T_b transistor are insignificant, and the power losses of the additional system are negligible.

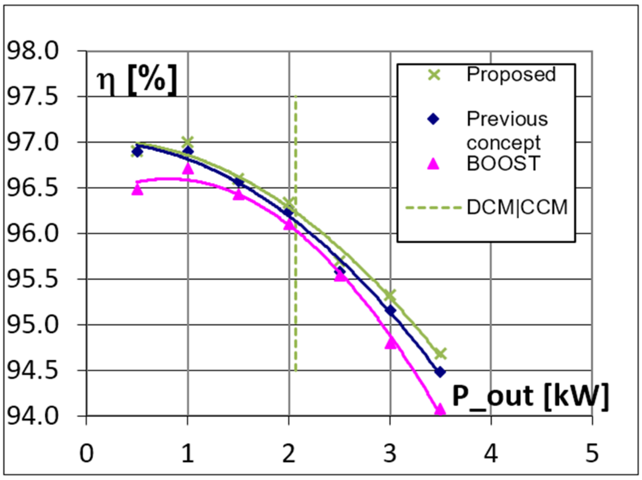

Figure 11. Efficiency vs. output power of the boost converter, the previous concept of the converter presented in Ref. [4], and the proposed circuit at the switching frequency f_{sw} = 32.2 kHz and the gain G_U = 4 (U_{in} = 100V, U_{out} = 400V).

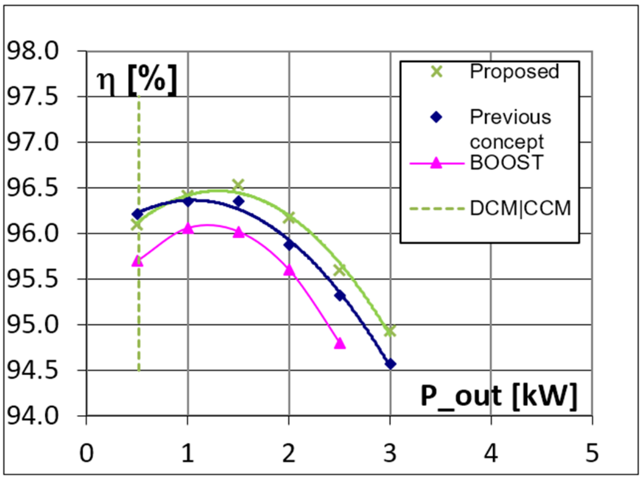

Figure 12. Efficiency vs. output power of the boost converter, the previous concept of the converter presented in Ref. [4], and the proposed circuit at the switching frequency f_{sw} = 48.7 kHz and the gain G_U = 4 (U_{in} = 100 V, U_{out} = 400 V).

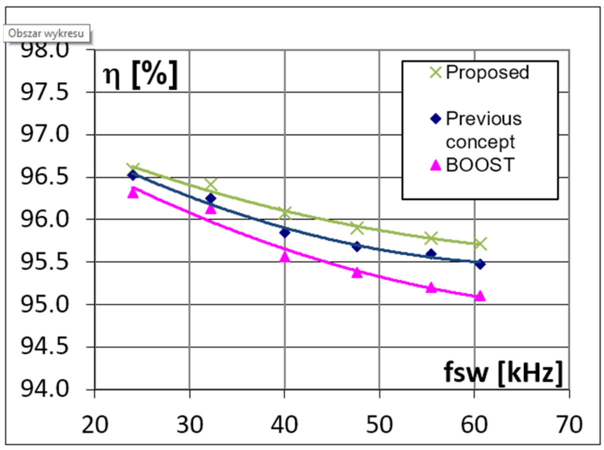

Figure 13. Efficiency vs. output power of the boost converter, the previous concept of the converter presented in Ref. [4], and the proposed circuit at the switching frequency P_{out} = 2 kW and the gain G_U = 4 (U_{in} = 100 V, U_{out} = 400 V).

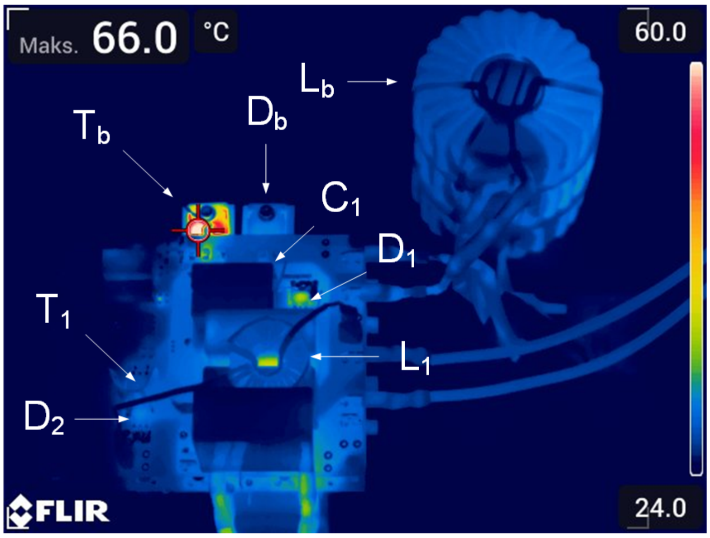

Figure 14. The IR photo for the proposed boost. V_{in} = 100 V; V_{out} = 400 V; P_{out} = 2 kW; f_{sw} = 32.2 kHz.

5. Conclusions

This article presents a new concept of turn-off power losses reduction in the boost converter for operation with voltage gain higher than two. The proposed auxiliary commutation circuit allows for ZVS during transistor turn-off. An active part of the auxiliary circuit assures its proper operation at high voltage gain.

It was shown that the proposed system has a higher efficiency than the classic IGBT-based boost converter. It was also shown that the new solution allows for higher efficiency than a reference circuit that implements soft switching in a way that is effective for gains lower than two.

The proposed system is relatively simple and uses a low number of components. Its control is synchronized with the switching of the main transistor. At low voltage gains the auxiliary circuit operates effectively as a passive circuit.

This article presents experimental results in the form of current and voltage waveforms as well as the results of heating the circuit obtained via thermal imaging measurement. From the heating results, it is clear that the most lossy element in the tested system is the IGBT transistor; therefore, reducing its losses is justified to obtain a more even distribution of losses in the real system.

The proposed system can be very advantageous in boost converter systems with IGBT transistors with high E_{off} energy lost during turn-off and allows for an increase in the switching frequency of the boost converter and a reduction in the volume of passive components.

Author Contributions: Conceptualization, S.P. and R.S; methodology, R.S. and A.M.; software, A.P.; formal analysis, S.P., R.S. and A.M; investigation, S.P., A.M., R.S, A.P. and P.G.; resources, R.S.; data curation; writing—original draft preparation, R.S., A.M. and A.P.; writing—review and editing, S.P., R.S., A.M., and P.G.; visualization, R.S., A.M., A.P. and P.G.; validation, S.P., R.S., A.M., A.P. and P.G.; supervision, R.S. and A.M.; project administration, R.S. and A.M. All authors have read and agreed to the published version of the manuscript.

Funding: This research received no external funding.

Data Availability Statement: Data sharing not applicable.

Conflicts of Interest: The author declare no conflict of interest. The funders had no role in the design of the study; in the collection, analyses, or interpretation of data; in the writing of the manuscript; or in the decision to publish the results.

References

1. Tofoli, F.L.; Pereira, D.d.C.; Josias de Paula, W.; Oliveira Júnior, D.d.S. Survey on non-isolated high-voltage step-up dc–dc topologies based on the boost converter. *IET Power Electron.* **2015**, *8*, 2044–2057. [CrossRef]
2. Berning, D.W.; Hefner, A.R. IGBT model validation for soft-switching applications. *IEEE Trans. Ind. Appl.* **2001**, *37*, 650–660. [CrossRef]
3. Gekeler, M.W. Soft switching three level inverter with passive snubber circuit (S3L inverter). In Proceedings of the 2011 14th European Conference on Power Electronics and Applications, Birmingham, UK, 30 August–1 September 2011.
4. Mondzik, A.; Stala, R.; Piróg, S.; Penczek, A.; Gucwa, P.; Szarek, M. High Efficiency DC–DC Boost Converter with Passive Snubber and Reduced Switching Losses. *IEEE Trans. Ind. Electron.* **2022**, *69*, 2500–2510. [CrossRef]
5. Stala, R.; Penczek, A.; Mondzik, A.; Szot, S.; Szarek, M.; Ryłko, M.S. Hochsetzsteller, Entsprechender Wechselrichter und Verfahren zur Verminderung von Ausschaltverlusten. Patent DE 102014119015B4, 23 June 2016.
6. Stala, R.; Penczek, A.; Mondzik, A.; Szot, S.; Szarek, M.; Ryłko, M.S. Voltage Increasing Converter, Appropriate Inverter and Method for Reducing the Trip-Out Losses. Patent PL 225731B1, 2017.
7. Willenberg, M.; Knoke, R.; Falk, A.; Stala, R.; Ryłko, M.; Masłoń, J.; Mondzik, A.; Szot, S.; Penczek, A.; Szarek, M. Step-Up Converter, Corresponding Inverter and Method of Operation. U.S. Patent 10491103 B2, 26 November 2019.
8. Gerber, D.; Biela, J. Interleaving of a Soft-Switching Boost Converter Operated in Boundary Conduction Mode. *IEEE Trans. Plasma Sci.* **2015**, *43*, 3374–3380. [CrossRef]
9. Yao, Z.; Lu, S. A Simple Approach to Enhance the Effectiveness of Passive Currents Balancing in an Interleaved Multiphase Bidirectional DC–DC Converter. *IEEE Trans. Power Electron.* **2019**, *34*, 7242–7255. [CrossRef]
10. Hsieh, Y.-C.; Hsueh, T.-C.; Yen, H.-C. An Interleaved Boost Converter with Zero-Voltage Transition. *IEEE Trans. Power Electron.* **2009**, *24*, 973–978. [CrossRef]
11. Van den Bossche, A.; Valtchev, V.; Ghijselen, J.; Melkebeek, J. Soft-switching boost converter for medium power applications. In Proceedings of the 1998 International Conference on Power Electronic Drives and Energy Systems for Industrial Growth, Perth, WA, Australia, 1–3 December 1998.
12. Choe, H.; Chung, Y.; Sung, C.; Yun, J.; Kang, B. Passive Snubber for Reducing Switching-Power Losses of an IGBT in a DC–DC Boost Converter. *IEEE Trans. Power Electron.* **2014**, *29*, 6332–6341. [CrossRef]
13. Lambert, J.A.; Vieira, J.B.; Carlos de Freitas, L.; dos Reis Barbosa, L.; Farias, V.J. A boost PWM soft-single-switched converter with low voltage and current stresses. *IEEE Trans. Power Electron.* **1998**, *13*, 26–35. [CrossRef]
14. Mohammadi, M.; Adib, E.; Yazdani, M.R. Family of Soft-Switching Single-Switch PWM Converters with Lossless Passive Snubber. *IEEE Trans. Ind. Electron.* **2015**, *62*, 3473–3481. [CrossRef]
15. Hua, G.; Leu, C.S.; Lee, F.C. Novel zero-voltage-transition PWM converters. In Proceedings of the PESC '92 Record. 23rd Annual IEEE Power Electronics Specialists Conference, Toledo, Spain, 29 June–3 July 1992; pp. 55–61.
16. Bodur, H.; Bakan, A.F. A new ZVT-PWM DC-DC converter. *IEEE Trans. Power Electron.* **2002**, *17*, 40–47. [CrossRef]
17. Gurunathan, R.; Bhat, A.K.S. A zero-voltage transition boost converter using a zero-voltage switching auxiliary circuit. *IEEE Trans. Power Electron.* **2002**, *17*, 658–668. [CrossRef]
18. Bodur, H.; Bakan, A.F. A new ZVT-ZCT-PWM DC-DC converter. *IEEE Trans. Power Electron.* **2004**, *19*, 676–684. [CrossRef]
19. Aksoy, I.; Bodur, H.; Bakan, A.F. A New ZVT-ZCT-PWM DC–DC Converter. *IEEE Trans. Power Electron.* **2010**, *25*, 2093–2105. [CrossRef]
20. Park, S.; Cha, G.; Jung, Y.; Won, C. Design and Application for PV Generation System Using a Soft-Switching Boost Converter With SARC. *IEEE Trans. Ind. Electron.* **2010**, *57*, 515–522. [CrossRef]
21. Li, Z.; Qian, W.; Zhang, X. An Optimized Zero-Voltage Zero-Current Transition Boost Converter Realized by Coupled Inductor. *IEEE Trans. Power Electron.* **2019**, *34*, 8882–8893. [CrossRef]
22. Qian, W.; Zhang, X.; Li, Z. Design and operation analysis of a novel coupled-inductor based soft switching boost converter with an auxiliary switch. In Proceedings of the 2016 IEEE 8th Int. Power Electron and Motion Control Conf. (IPEMC-ECCE Asia), Hefei, China, 22–26 May 2016.
23. Akın, B. An Improved ZVT–ZCT PWM DC–DC Boost Converter with Increased Efficiency. *IEEE Trans. Power Electron.* **2014**, *29*, 1919–1926. [CrossRef]
24. Altintaş, N.; Bakan, A.F.; Aksoy, İ. A Novel ZVT-ZCT-PWM Boost Converter. *IEEE Trans. Power Electron.* **2014**, *29*, 256–265. [CrossRef]
25. Tseng, C.-J.; Chen, C.-L. Novel ZVT-PWM converters with active snubbers. *IEEE Trans. Power Electron.* **1998**, *13*, 861–869. [CrossRef]
26. Huang, W.; Moschopoulos, G. A new family of zero-voltage-transition PWM converters with dual active auxiliary circuits. *IEEE Trans. Power Electron.* **2006**, *21*, 370–379. [CrossRef]
27. Huang, W.; Gao, X.; Bassan, S.; Moschopoulos, G. Novel dual auxiliary circuits for ZVT-PWM converters. *Can. J. Electr. Comput. Eng.* **2008**, *33*, 153–160. [CrossRef]
28. Park, S.; Park, S.; Yu, J.; Jung, Y.; Won, C. Analysis and Design of a Soft-Switching Boost Converter With an HI-Bridge Auxiliary Resonant Circuit. *IEEE Trans. Power Electron.* **2010**, *25*, 2142–2149. [CrossRef]
29. Tran, H.N.; Choi, S. A Family of ZVT DC–DC Converters with Low-Voltage Ringing. *IEEE Trans. Power Electron.* **2020**, *35*, 59–69. [CrossRef]

30. Bauman, J.; Kazerani, M. A Novel Capacitor-Switched Regenerative Snubber for DC/DC Boost Converters. *IEEE Trans. Ind. Electron.* **2011**, *58*, 514–523. [CrossRef]
31. Mishima, T.; Takeuchi, Y.; Nakaoka, M. Analysis, Design, and Performance Evaluations of an Edge-Resonant Switched Capacitor Cell-Assisted Soft-Switching PWM Boost DC–DC Converter and Its Interleaved Topology. *IEEE Trans. Power Electron.* **2013**, *28*, 3363–3378. [CrossRef]
32. Jang, Y.; Jovanovic, M.M. A new, soft-switched, high-power-factor boost converter with IGBTs. *IEEE Trans. Power Electron.* **2002**, *17*, 469–476. [CrossRef]
33. Bodur, H.; Yıldırmaz, S. A New ZVT Snubber Cell for PWM-PFC Boost Converter. *IEEE Trans. Ind. Electron.* **2017**, *64*, 300–309. [CrossRef]
34. Cetin, S. Power-Factor-Corrected and Fully Soft-Switched PWM Boost Converter. *IEEE Trans. Ind. Appl.* **2018**, *54*, 3508–3517. [CrossRef]